Quantal version of resonance overlap

1987 J. Phys. A: Math. Gen. 20 3833

(http://iopscience.iop.org/0305-4470/20/12/031)

J. Phys. A: Math. Gen. **20** (1987) 3833-3847. Printed in the UK

Quantal version of resonance overlap

M Toda† and K Ikeda‡

† Department of Physics, Kyoto University, Kyoto 606, Japan
‡ Research Institute for Fundamental Physics, Kyoto University, Kyoto 606, Japan

Received 23 October 1986, in final form 11 December 1986

Abstract. A quantal version of resonance overlap leading to global chaos is investigated. Classical chaos is reflected in irregular features of quantum beats in the phase space profile of eigenfunctions. These quantum beats are due to interference between nearby branches of bifurcated classical manifolds. Statistical properties of the quantum system qualitatively reflect the classical transition to global chaos although some discrepancies from classical ergodicity are found in the quantum mechanics even in the fully chaotic regime.

1. Introduction

The understanding of classical chaos has developed greatly since Poincaré demonstrated the non-integrability of the three-body problem. The famous mathematical work by Kolmogorov, Arnold and Moser (KAM) has established the condition for the existence of tori in formally non-integrable systems. These tori are now called KAM tori. However, the criterion for the occurrence of global chaos is a difficult problem to solve mathematically. On the other hand a physical criterion has been established by Chirikov (1979). He proposed that an overlap of two domains of resonances gives rise to globally chaotic behaviour. This is a universal mechanism leading to global chaos. The detailed classical mechanism of resonance overlap has been investigated by various authors in the past ten years (Greene 1968, 1979, Escande and Doveil 1981, Lichtenberg and Lieberman 1983).

On the other hand, quantal aspects of chaotic behaviour are still controversial questions although some pioneering work has been done. The first question concerning semiclassical quantisation in non-integrable systems was raised by Einstein (1917). He proposed a quantisation condition based on tori, the existence of which were later the subject of the KAM theory. However the characteristics of eigenfunctions when KAM tori are entirely destroyed have not been understood yet. Recently certain irregularities in energy levels and eigenfunctions have been called 'quantum chaos'. The distribution of energy levels becomes irregular when the classical version of a system goes into a chaotic regime (Percival 1973). In such a chaotic regime energy spectra exhibit complicated anti-crossing and the level spacings obey the Wigner distribution (Berry 1981). Furthermore eigenfunctions in a chaotic regime are characterised by complicated nodal lines (McDonald and Kaufman 1979). However it is quite unclear how these features of 'quantum chaos' are related to the stochastic behaviour of corresponding classical systems. Moreover, it is known that there exists an important discrepancy between quantum and classical dynamics in a chaotic regime. In a study of the quantum version of the standard map, Casati *et al* (1979) found that the diffusive motion inherent

0305-4470/87/123833+15$02.50

in the classical chaos is limited within a finite timescale for the quantum system. Such a limitation has been discussed in terms of Anderson localisation (Fishman *et al* 1982, Grempel *et al* 1984).

Although quantal aspects of chaotic behaviour have been investigated for various systems, resonance overlap has not been studied in detail quantum mechanically. As mentioned above, resonance overlap is a universal mechanism leading to global chaos. Therefore the understanding of a quantum version of resonance overlap will provide a universal picture of global chaos in quantum mechanics. The standard map is one model which exhibits global chaos due to resonance overlap. However, in the standard map it is impossible to isolate an elementary process of resonance overlap, since too many resonances are involved. Therefore more idealised systems should be studied.

In this paper we aim to elucidate a quantum version of resonance overlap from various points of view. For this purpose we choose an ideal system which exhibits an overlap of resonances and investigate the following questions. (i) Do quantum systems exhibit certain kinds of randomness that are related to the stochastic behaviour of the corresponding classical systems? (ii) How do the phase space profiles of eigenfunctions reflect the breakup of KAM tori and the breakdown of the EBK quantisation? (iii) Do quantum systems have statistical properties that reflect the ergodicity of corresponding classical systems?

We summarise the contents of the following sections. In § 2 we introduce our model and survey briefly its classical behaviour. In § 3 we study how the characteristics of the eigenfunctions projected onto the action space (§ 3.1) and onto the phase space (§ 3.2) vary with the advance of resonance overlap. In particular, we discuss in § 3.2 the relation between the phase space profile of each eigenfunction and the structure of the classical phase space. General characteristics of the eigenfunctions are revealed in statistical properties of transition probabilities. These are discussed in § 4 to make manifest how classical ergodicity is reflected in the quantum system. Section 5 is devoted to the conclusions of our paper and suggestions for further study. The details of our numerical procedure are explained in the appendix.

2. The model

Our model is described by the following Hamiltonian, which we call the double resonance model (DRM):

$$H = \hat{I}^2/2 + V_1 \cos\theta + V_2 \cos(\theta - \omega t) \tag{1}$$

where $\hat{I} \equiv -i\partial/\partial\theta$ and θ are the canonical conjugate variables which classically correspond to the action and angle variables, respectively. We normalise our Hamiltonian in such a way that the Planck constant $\hbar$ is included in the frequency ω of the driving force and in the coupling constants V_i $(i = 1, 2)$, so that $\omega \propto \hbar^{-1}$ and $V_i \propto \hbar^{-2}$.

We choose the DRM because of the following reasons: as will be explained later, the classical version involves only a single pair of primary resonances, and so it describes an idealised process of overlap of resonances leading to globally chaotic behaviour. Therefore this system is appropriate for studying the elementary process of the global stochastisation quantum mechanically. There is also a computational merit. Since the classical region of chaotic behaviour is bounded in the phase space, the number of quantum orthogonal functions demanded to span the chaotic region is finite. Furthermore, this system is free from Anderson localisation, which is peculiar

to unbounded chaotic systems such as the standard map. Therefore, we can study ideal features of the semiclassical correspondence in resonance overlap.

Next we give a brief survey of the behaviour of the classical DRM. The model has two primary resonances in the vicinity of $I=0$ and $I=\omega$. Within each primary resonance domain we can approximate the DRM by the single resonance Hamiltonian $H_s=\hat{I}^2/2+V_i\cos\theta$ $(i=1,2)$. In the domain of each resonance classical orbits are trapped to form elliptic orbits, and they are enclosed by the separatrix orbit $I=I_i\pm 2\sqrt{V_i}\sin(\theta/2)$ ($i=1, 2$, and $I_1=0$, $I_2=\omega$). When the overlapping parameter defined by

$$S\equiv 2(\sqrt{V_1}+\sqrt{V_2})/\omega \tag{2}$$

is small, most of the phase space between the two primary resonances is filled with tori corresponding to rotational orbits. Chaotic orbits exist because of the heteroclinic structure of the separatrix orbits. However, they are not extended in the phase space. They cling to the separatrix orbits. With an increase in S the stochastic layers around the two primary resonances grow. When S exceeds the threshold value $S_c\sim 0.71$, they overlap and eventually tangle together to form global chaos which connects the two resonance domains (Escande and Doveil 1981).

In figure 1(b), we show the cross section of orbits (the Poincaré map) obtained at every period $\tau=2\pi/\omega$ of the driving force. The Poincaré maps are shown for the three representative values of S, i.e. $S=0.6$, 0.8 and 1.0. $S=0.6$ is below the threshold of global stochastisation. Most of the phase space is filled with tori and there exists a hierarchy of elliptic orbits trapped by the primary and higher-order resonances with rational winding numbers $I=(m/n)\omega$. Resonances with simple rational winding numbers ($n=1, 2, 3$ and 4, $m=1$) are indicated by arrows. $S=0.8$ is just above the threshold. Stochastic layers around the two primary resonances have already overlapped to form global chaotic orbits. However, a considerable portion of the phase space is still occupied by the non-stochastic islands composed of the stable elliptic orbits. The islands due to the primary resonances ($I=0, \omega$) and due to the one-half resonance ($I=\omega/2$) are particularly noticeable. $S=1.0$ is sufficiently far above the threshold. The phase space is almost completely covered with global chaotic orbits except for the small non-stochastic islands due to the two primary resonances.

In the following we investigate how the global stochastisation classically described above emerges in quantum mechanics. To investigate the quantum motion described by the Schrödinger equation $\mathrm{i}\partial\psi/\partial t=H(t)\psi$ we construct a stroboscopic transformation defined for the interval τ:

$$U\equiv T\exp\left(-\mathrm{i}\int_0^{\tau}H(t')\,\mathrm{d}t'\right) \tag{3}$$

where T is a time-ordering operator. This transformation corresponds to the Poincaré map of the classical system. Once the sets of eigenfunctions $\{\phi_k(\theta)\}$ and eigenvalues $\{\exp(\mathrm{i}\varepsilon_k)\}$ of the unitary operator U are obtained, wavefunctions $\psi_n\equiv\psi(\theta, n\tau)$ at the nth step are expressed in terms of the initial state ψ_0 as

$$\psi_n(\theta)=\sum_k \exp(\mathrm{i}\varepsilon_k n)\langle\phi_k|\psi_0\rangle\phi_k(\theta). \tag{4}$$

From now on we assume $V_1=V_2=V$ for the sake of simplicity. Then our system is specified by only two parameters S and ω, the latter being the quantal parameter proportional to $\hbar^{-1}$. We briefly comment on the symmetry properties of the DRM.

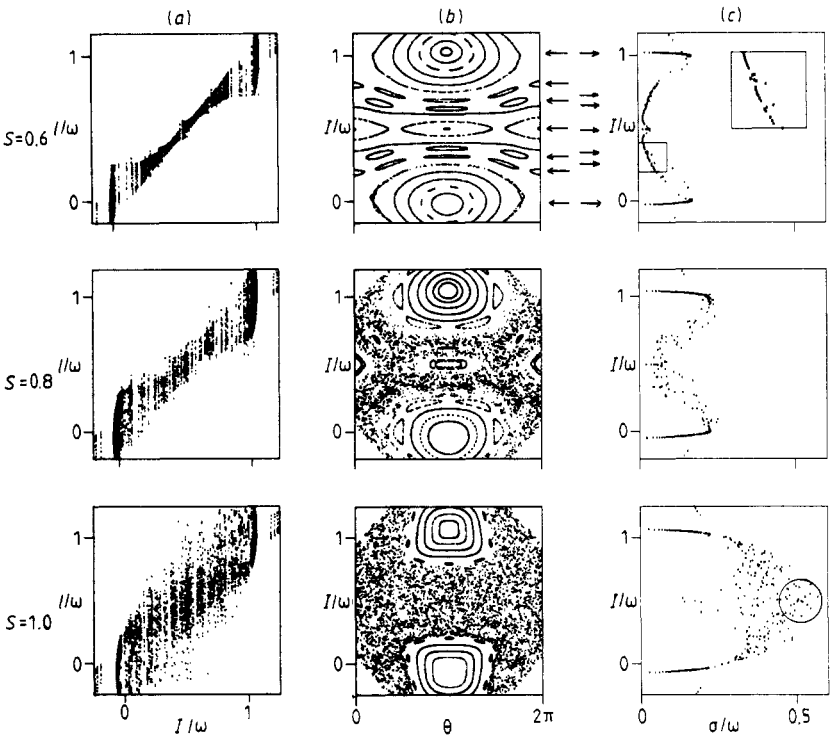

Figure 1. (*a*) Localisation diagram, (*b*) classical Poincaré map and (*c*) (I, σ) plot below the threshold ($S = 0.6$), just above the threshold ($S = 0.8$) and sufficiently far above the threshold ($S = 1.0$). Here $\omega = 160.3$. The arrows at $S = 0.6$ indicate the self-similarity of the trapped elliptic orbits (*b*) and the corresponding clustered structures of the (I, σ) plot (*c*). The inset magnifies the clusters enclosed in the square to make the hierarchy of the (I, σ) plot manifest. At $S = 1.0$ global eigenfunctions which extend over the whole of the chaotic region are encircled in the (I, σ) plot.

When $V_1 = V_2$, the classical system is invariant under the canonical transformation defined by the generating function $S(\theta', I, t) = -(\omega - I)\theta' - \omega t I$. This is an inversion round $I = \omega/2$. However, the quantum system has the same symmetry only when ω agrees with an eigenvalue of the operator $\hat{I}$, i.e. an integer. In this case resonant quantum tunnelling occurs between the two primary resonances. This phenomenon also occurs in the case of the standard map. To avoid such a phenomenon, which is irrelevant to our study of classical-quantum correspondence, we always choose ω to be non-integral.

3. Characteristics of eigenfunctions

In this section we investigate how the characteristics of the eigenfunctions $\{\phi_k\}$ of the unitary operator U vary as the overlap of resonances advances with an increase in S.

As S increases, classical orbits which are localised in the action space become delocalised and finally collapse into global chaotic orbits connecting the two resonances which were separated in the action space. Such properties should be most directly reflected in the localisation characteristics of eigenfunctions projected onto the action space. This will be investigated in § 3.1.

If S is not too large, most of the classical phase space is filled with tori and the quantisation of tori is achieved according to the Einstein-Brillouin-Keller (EBK) rule. This implies that the profiles of eigenfunctions projected onto the phase space should have their counterparts in classical orbits. However, as S increases, most of the tori are destroyed and the EBK quantisation can no longer be applied. How do the profiles of the eigenfunctions change in such a regime? How are they related to the structure of the classical phase space? These problems are studied in § 3.2.

3.1. Characteristics in action space

In figure 1(a), we present localisation diagrams which indicate the localisation characteristics of eigenfunctions. In these diagrams the abscissa indicates the eigenfunctions characterised by the mean action

$$I_k \equiv \sum_{l=-\infty}^{\infty} l P_k(l) \tag{5}$$

where $P_k(l) \equiv |\langle u_l|\phi_k\rangle|^2$ stands for the weight of ϕ_k projected onto an action eigenfunction $u_l(\theta) \equiv \exp(il\theta)/\sqrt{2\pi}$ (l is an integer). The ordinate indicates the action eigenvalue l. The lines indicate the domains of l at which ϕ_k satisfies $P_k(l) \geqslant 0.02$. The localisation diagrams are presented for the three representative values of S, i.e. $S = 0.6$, 0.8 and 1.0, each of which is compared with the corresponding classical Poincaré map.

At $S = 0.6$ most of the eigenfunctions are localised in quite small regions in the action space and the width of each eigenfunction agrees quite well with the range of the projection of the corresponding classical orbit onto the action axis. Thus the classical-quantum correspondence holds good in this case. As S exceeds S_c, each eigenfunction gradually tends to extend. However, its width is not large enough to cover the range in the action space connected by the classical global chaos. Such a discrepancy is particularly marked at $S = 0.8$.

To describe the above features more quantitatively, we introduce another diagram. Define the localisation width σ_k of an eigenfunction ϕ_k as

$$\sigma_k^2 \equiv \sum_{l=-\infty}^{\infty} (l - I_k)^2 P_k(l). \tag{6}$$

We plot all the points specified by (I_k, σ_k) on a single two-dimensional plane. We call such a diagram the I-σ plot. Examples for the three representative values of S are shown in figure 1(c).

At $S = 0.6$ the phase space is almost entirely filled with the invariant tori (figure 1(b)). Arrows indicate tori inside the domains of the primary resonances ($I = 0, \omega$) and of the higher-order resonances ($I = (m/n)\omega$; $n = 2, 3$ and 4, $m = 1$). These orbits are quantised and the corresponding plots are clustered as indicated by arrows in figure 1(c). Therefore, the classical self-similar structure of resonances is reflected in the existence of various scales of clustered structures in the I-σ plot. Except for the clustered points, most of the points lie along a definite smooth curve. They correspond to the classical rotational orbits flowing between the resonances. The existence of the smooth curve in the I-σ plot implies that there exists a good quantum number.

At $S = 0.8$, the last KAM torus has already been destroyed and global chaos has appeared in the classical system. Correspondingly, the localisation widths of the eigenfunctions are larger than those at $S = 0.6$. However, they are still too small to

connect the two primary resonances. It should be noted that the pattern in the I-σ plot has lost its smooth structure and become slightly irregular, which implies that the tori are damaged and have become 'vague tori' (see § 3.2).

At $S = 1.0$ any structures between the two primary resonances disappear and the stochastic sea covers the greater part of the classical phase space. Correspondingly, the widths of some eigenfunctions grow large enough to connect the two primary resonances. Such eigenfunctions are 'ergodic' and lose their individuality in the sense that they cannot be characterised by I_k. Indeed, points in figure 1(c) corresponding to these functions are all distributed along the centre line of the two primary resonances, i.e. $I = \omega/2$, which are enclosed by a circle in figure 1(c). However, the relative number of such eigenfunctions is quite small (about 15% for $\omega = 160.3$). Other eigenfunctions are not 'ergodic' and they do not lose their individuality in the sense that they can roughly be specified by their I_k. Their widths are not large enough to connect the two primary resonances. At $S = 1.0$ all the plotted points, except for those in the clusters corresponding to the elliptic orbits trapped by the two primary resonances, are scattered in a quite irregular manner and no structure can be seen in the I-σ plot. This implies that a good quantum number does not exist.

3.2. Characteristics in phase space

A number of representations have been proposed which project a quantum wavefunction onto a momentum ($\boldsymbol{p}$)-position ($\boldsymbol{q}$) phase space. One of the most famous representations is the Wigner function which is defined by

$$W(\boldsymbol{p}, \boldsymbol{q}) = \int \exp(2i\boldsymbol{p}\boldsymbol{r}/\hbar)\psi(\boldsymbol{q}-\boldsymbol{r})\psi^*(\boldsymbol{q}+\boldsymbol{r})\,d\boldsymbol{r}/(\pi\hbar)^n \tag{7}$$

where $\psi(\boldsymbol{q})$ is the quantum wavefunction to be represented (Berry 1977a, Korsh and Berry 1981). This representation has, however, several defects. It may be negative and, moreover, it is accompanied by rapid oscillations of the de Broglie wavelength. To eliminate such undesirable properties, we have to process the Wigner function by an appropriate coarse graining (Takahashi and Saito 1985).

Instead of the Wigner function we use the diagonal representation

$$Q(\boldsymbol{p}, \boldsymbol{q}) = |\langle\psi|\boldsymbol{p}, \boldsymbol{q}\rangle|^2 \tag{8}$$

with respect to the coherent state† $|\boldsymbol{p}, \boldsymbol{q}\rangle$, which is an eigenstate of the annihilation operator $\boldsymbol{a} = (\boldsymbol{p} - i\boldsymbol{q})/\sqrt{2\hbar}$ with an eigenvalue $(\boldsymbol{p} - i\boldsymbol{q})/\sqrt{2\hbar}$. This function is a probability distribution function which is non-negative and non-singular. Moreover, it is free from the rapid de Broglie oscillation, because its definition automatically involves a sort of coarse graining operation. We now investigate the phase space profile of eigenfunctions at the three representative values of S using the distribution function $Q(I, \theta)$.

3.2.1. $S = 0.6$—quantised KAM tori. The I-σ plot in figure 1 implies that there exists a good quantum number which specifies a series of KAM tori. Indeed, the phase space profiles of the eigenfunctions agree quite well with the classical orbits in the Poincaré map. We show some examples in figure 2(a). These are quantised libration orbits

† The coherent state has arbitrariness of squeezing. However, the arbitrariness does not matter at all as long as it is not extremely squeezed compared with the classical phase space structure.

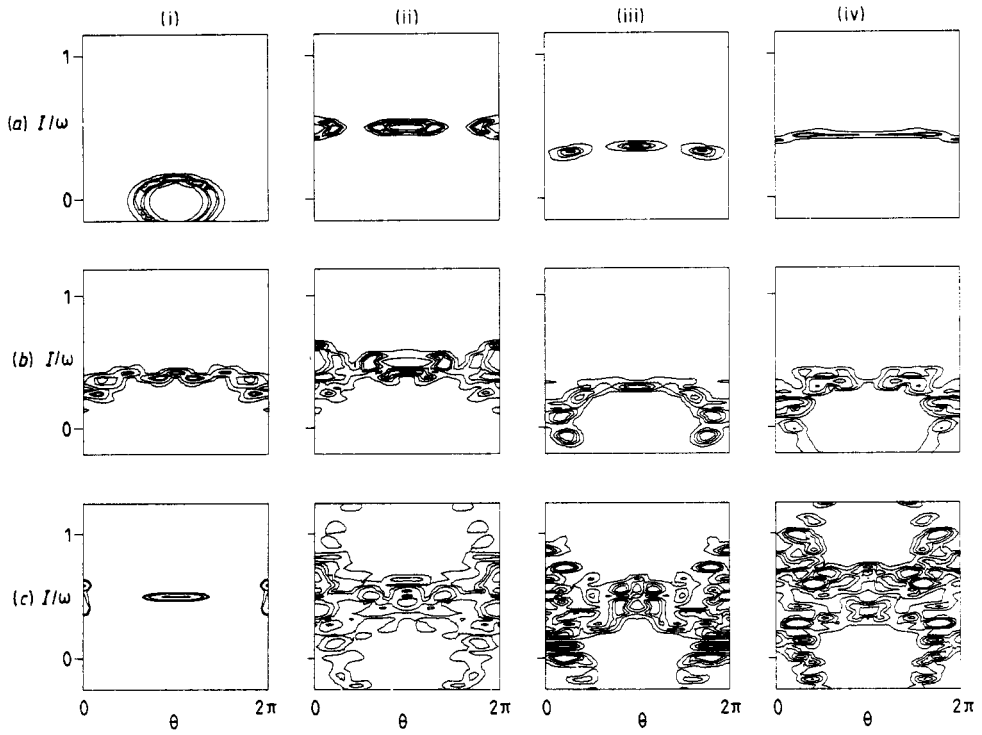

Figure 2. Typical examples of the phase space profile of eigenfunctions at three values of S. (*a*) $S = 0.6$, (*b*) $S = 0.8$ and (*c*) $S = 1.0$. Here $\omega = 160.3$. Contour lines are drawn so that the net probability inside of each contour equals 0.3, 0.5, 0.7 and 0.9, respectively. See the text for explanation of (i)-(iv).

trapped by the primary, (i), and higher-order, (ii) and (iii), resonances and a quantised rotation orbit, (iv). Below the threshold, most of the eigenfunctions have their counterparts in classical tori. Thus a hierarchy of eigenfunctions exists, which corresponds to the self-similar structure of the classical phase space. There is the limitation due to the uncertainty principle; the quantum counterpart of classical structure finer than $\hbar$ cannot exist.

3.2.2. $S = 0.8$—quantised 'vague tori'. As expected from the I-σ plot, no eigenfunction spreads over the classical chaotic region, although the overlapping parameter S exceeds the threshold of the global stochastisation. The reason is as follows: for S slightly larger than S_c, although the global chaos surely exists, classical chaotic trajectories are confined in tori for finite time intervals (Jaffé and Reinhardt 1982, Shirts and Reinhardt 1982). In other words, classical tori exist with finite lifetimes. They are partially damaged and entangle with each other in a complicated manner within small regions of the phase space to form global chaotic orbits. The quantum system, however, cannot be affected by the existence of such a tangle if its area is smaller than the Planck constant $\hbar$. In other words, quantum mechanics repairs the damaged tori. Thus the quantised orbits still possess the characteristics of tori. They are what Reinhardt and colleagues call 'vague tori'.

However, the quantised 'vague tori' are qualitatively different from the quantised KAM tori. Quantisation on a KAM torus is done in such a way that the phase gains of

a wavefunction around closed paths on a torus are integer multiples of 2π (the EBK condition). The classical tori above the stochastisation threshold are damaged and are bifurcated into multiple branches. To make approximately closed paths on a 'vague torus' we have to pass through some of the bifurcated branches. The wavefunctions on nearby branches interfere with each other to form slowly varying beats along the phase space profile of eigenfunctions, as shown in figure 2(b). The pattern of lumps due to such beats reflects the complicated nature of damaged tori.

3.2.3. $S = 1.0$—random quantum interference. At $S = 1.0$ most of the eigenfunctions lose the shape of 'vague tori'. Compared with the case of $S = 0.8$, lumps due to quantum interference are distributed much more irregularly over much wider regions. This is attributed to the appearance of complicated global manifolds on which classical chaotic orbits are trapped (see figure 3; this is an example of an unstable manifold originating from a hyperbolic point). Let us try to construct a wavefunction on a chaotic manifold just as is done on a torus. The chaotic manifold has a much more complicated structure, composed of infinitely multiplicate branches. Such a structure is formed by repetitions of stretching and folding which are inherent in chaotic dynamics. Along a branch of the manifold the phase of a wavefunction varies continuously, but the phases on the nearby branches are random with respect to each other. Thus the wavefunction interferes with itself everywhere on the branches of the chaotic manifold to form lumps randomly distributed over the phase space region occupied by the chaotic manifold. The possibility of such characteristics has also been conjectured by Berry (1977b).

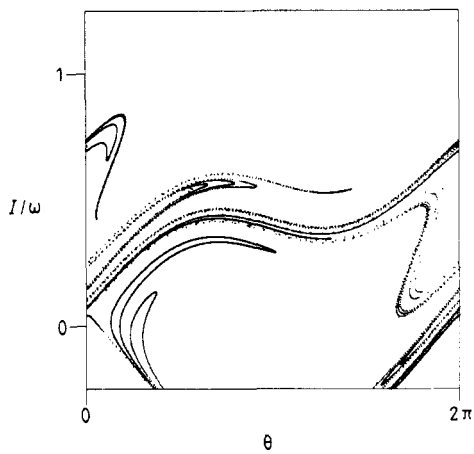

Figure 3. Phase portrait of a complicated global manifold on which classical chaotic orbits are trapped at $S = 1.0$.

Although the eigenfunctions exhibit these random features, only a few of them extend over the classical stochastic sea, as we mentioned in § 3.1. We show in figure 2(c), (i)-(iv), the prototypes of the phase space profile of the eigenfunctions. Their relative numbers are shown for $\omega = 160.3$. Their explanation is as follows.

(i) An example of quantised elliptic orbits trapped in the domain of one-half resonance (about 5%). The quantised elliptic orbits still exist in the domain of the primary resonances. However, it is quite surprising that a quantised elliptic orbit still

remains in the domain of one-half resonance, which classically has disappeared into the stochastic sea (figure 1(*b*)). This fact implies an anomalous stability of quantum systems (Heller 1984). Except for these eigenfunctions all others appear to be quite random.

(ii) An example of an eigenfunction which spreads over the one-half resonance (about 20%).

(iii) An example of an eigenfunction which connects the primary resonance and the one-half resonance (about 30%).

(iv) An example of an eigenfunction which extends over the whole region of the classical stochastic sea (about 15%).

Other eigenfunctions extend only over one or other of the primary resonances (about 30%). The relative number of 'ergodic' eigenfunctions (iv) gradually increases with a decrease of the Planck constant $\hbar$. This implies the recovery of the classical ergodicity. We discuss this problem in detail in § 4.

4. Statistical properties

In the previous section we have shown that all the eigenfunctions of the unitary operator U are not 'ergodic' even in the fully chaotic regime. In this section we study how the statistical properties of the quantum system qualitatively reflect the transition to global chaos. In particular we elucidate the quantitative disagreement between the classical and the quantum systems in the fully chaotic regime.

Let $|i\rangle$ and $|f\rangle$ be initial and final states, respectively. When there is no degeneracy in the quasi-energy spectra of the unitary operator U, then

$$C(i|f) = \sum_k |\langle i|\phi_k\rangle|^2 |\langle f|\phi_k\rangle|^2 \tag{9}$$

describes the long time average of the probability that the system starting from the initial state $|i\rangle$ is found in the state $|f\rangle$.

In integrable systems each eigenfunction has its counterpart in a classical torus and the quantal probability density $C(i|f)$ agrees in the semiclassical limit with the long time average of the probability of the classical trajectory staying on the corresponding torus. Therefore, $C(i|f)$ of integrable systems can be predicted by their classical behaviour. In particular, $C(i|f)$ depends significantly on whether the initial state $|i\rangle$ and the final one $|f\rangle$ are on the same torus or not. If not, a contribution to the probability comes from quantum tunnelling, which has an exponential dependence on the Planck constant $\hbar$ and approaches zero rapidly in the semiclassical limit. Such non-ergodic features are characteristic of integrable systems.

In chaotic classical systems all tori in the stochastic sea are completely destroyed. A classical trajectory starting from a particular initial state chosen in the stochastic sea travels over the whole of the stochastic sea and loses its initial memory after a lapse of sufficiently long time. Provided that the classical behaviour can predict the quantum probability distribution, $C(i|f)$ should be independent of both $|i\rangle$ and $|f\rangle$ if they are chosen in the stochastic sea. However, the results in the previous section imply that this is not the case.

Roughly speaking, for $S > S_c$ the phase space consists of two regions, i.e. the stochastic sea and the non-stochastic islands. The boundary of the stochastic sea around the primary resonance is approximated by a classical orbit of the single

resonance Hamiltonian

$$H_S = \tfrac{1}{2}\hat{I}^2 + V\cos\theta \tag{10}$$

with an appropriate energy $H_S = E_B$, i.e.

$$I = \pm\sqrt{2}(E_B - V\cos\theta). \tag{11}$$

Let us choose the initial state $|i\rangle$ to be an eigenstate of H_S specified by an energy eigenvalue E_S, i.e. $H_S|E_S\rangle = E_S|E_S\rangle$. If E_S is much larger than E_B, the corresponding classical orbit is entirely contained in the stochastic sea, while it is contained in the non-stochastic island if $E_S \ll E_B$. Therefore, by increasing E_S from its classical lower bound $-V$, the initial state can be moved from the inside of the non-stochastic island through the boundary orbit into the stochastic sea (figure 4). We choose a final state $|f\rangle$ to be an action eigenstate.

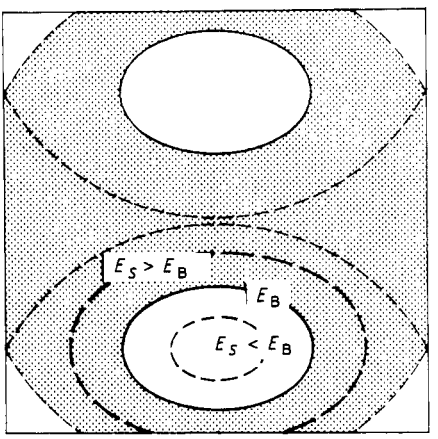

Figure 4. Schematic diagram illustrating the boundary between the stochastic sea and the non-stochastic islands. The bold broken curves are classical orbits of H_S. For $E_S > E_B$ they are entirely in the stochastic sea, while they are contained in the non-stochastic island for $E_S < E_B$. The short broken curves indicate the separatrix orbits. The shaded area represents the chaotic region.

First we show in figure 5 the shape of $C(E_S|I)$ at three representative values of S when an initial state is entirely contained in the stochastic regions. Here we choose the separatrix orbit ($E_S = V$) as the initial state because the vicinity of the separatrix is always occupied by the stochastic layers. The quantal distributions agree or disagree with the classical ones in the following manner. On a logarithmic scale the shape of $C(E_S|I)$ looks like a plateau. The plateau consists of two steps with different heights and each of the steps spreads over the domain of one of the primary resonances. These steps are due to the elliptic motions in the resonance domain and such flat steps also exist for the classical probability distribution. As the domains of the two primary resonances are separated by KAM tori for $S < S_C$, the difference in the step height is expected at $S = 0.6$. However for $S > S_C$, whereas in the classical case the step difference should disappear, it remains quite large for the quantum distribution. In particular, a notable difference exists just above S_C. At $S = 0.8$ the ratio of heights is estimated 10^4-10^5 for $\omega(\propto \hbar^{-1}) \sim 10^2$. The difference decreases with an increase in S, but it remains significant even at $S = 1.0$.

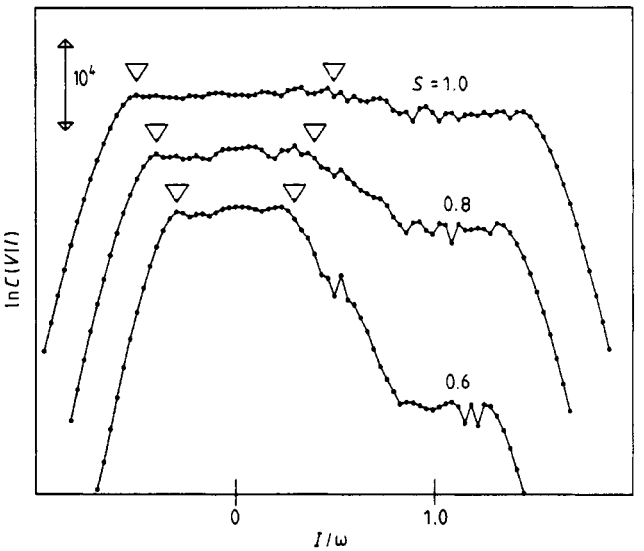

Figure 5. The shape of $C(E_S = V|I)$ on a logarithmic scale at three values of S. ∇ indicates the range of the separatrix orbit projected onto the action space. Here $\omega = 30.3$.

To see more clearly the disagreement with the classical ergodic behaviour in the chaotic regime, we study how the quantal probability distribution $C(i|f)$ depends on the initial state as we vary the Planck constant. For $S > S_C$, we can, by varying E_S, bring an initial state from the inside of the non-stochastic island to the stochastic sea across the boundary with energy E_B. Then classical probability distributions in the vicinity of the second primary resonance ($I \sim \omega$) should increase steeply from zero to some finite value as E_S exceeds E_B. For the quantum system, let us introduce an integrated probability in the vicinity of the second primary resonance

$$\bar{C}(E_S, \omega) \equiv \sum_{|\omega - I| \leq \Delta} C(E_S|I) \tag{12}$$

where the width Δ is chosen to be an appropriate value comparable to the width of the primary resonance, i.e. $\Delta \sim \sqrt{V}$. In figure 6 we show the initial state dependence of $\bar{C}(E_S, \omega)$ for various values of $\omega \propto \hbar^{-1}$. $\bar{C}(E_S, \omega)$ exhibits a transition which is qualitatively similar to that anticipated classically. For $E_S < E_B$ the logarithm of $\bar{C}(E_S/\omega)$ varies linearly with the initial state. Moreover, it decreases in proportion to the Planck constant. These facts imply that the probability leaks out of the domain of the first primary resonance by quantum tunnelling. Indeed, the magnitude of $\bar{C}(E_S, \omega)$ is roughly explained by the tunnelling probability through KAM tori between the two primary resonances (Ikeda and Toda 1983).

As E_S exceeds E_B the initial state dependence of $\bar{C}(E_S, \omega)$ changes from that for $E_S < E_B$. Further, $\bar{C}(E_S, \omega)$ varies with the decrease of the Planck constant in a quite different manner. This implies that a pure quantum mechanism is replaced by a certain classical one. However, just above the threshold, the magnitude of $\bar{C}(E_S, \omega)$ is much less than that expected from the classical ergodicity. Moreover, the initial state dependence is irregular especially in the vicinity of the separatrix and the magnitude is scattered in the logarithmic scale. These irregularities are amplified as the Planck constant gets smaller. In addition, $\bar{C}(E_S, \omega)$ does not seem to tend toward the classical ergodicity with the decrease of the Planck constant. It varies quite irregularly and its

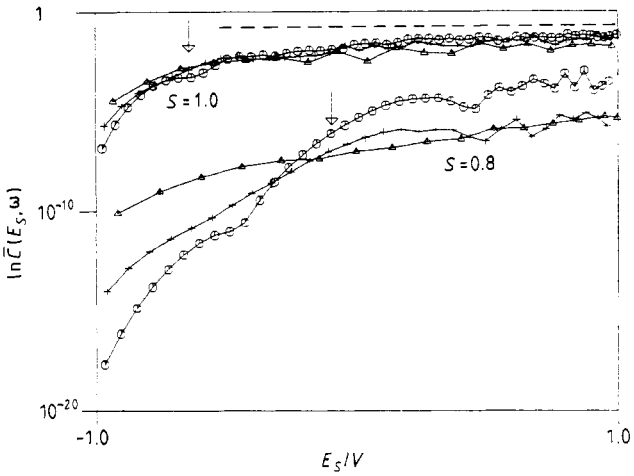

Figure 6. The dependence of $\bar{C}(E_S, \omega)$ on the initial state is shown on a logarithmic scale. The broken line is the classically expected value. The arrows indicate the boundary energy E_B. $\omega = 30.3$ (△), 60.3 (+), 80.3 (◯).

variance ranges over the logarithmic scale (see figure 7(*a*)). This is explained in terms of 'vague tori': The spread of the 'vague tori' is not wide enough to connect the two primary resonances although they are more extended than the KAM tori. Therefore the two resonances are connected by the tail of the localised eigenfunctions corresponding to 'vague tori'. In addition, these eigenfunctions exhibit irregular features due to quantum beats. These irregularities are revealed in the transition probability especially for the initial states in the vicinity of the separatrix owing to the existence of the stochastic layer. Furthermore, their dependence on the Planck constant is quite irregular in the semiclassical limit reflecting the bifurcated multiple branches of damaged classical tori. Such irregularities are exponentially amplified at the tail of

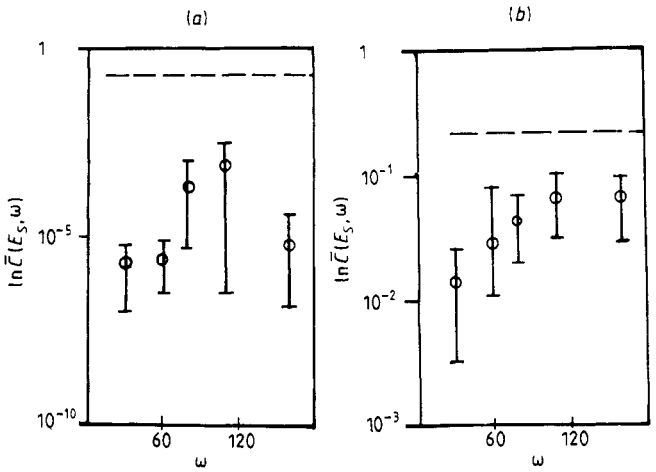

Figure 7. Dependence of $\bar{C}(E_S, \omega)$ on $\omega \propto \hbar^{-1}$. The average of $\bar{C}(E_S, \omega)$ over $0 \leq E_S \leq V$ is plotted on a logarithmic scale. The error bars indicate the maximum and minimum values of $\bar{C}(E_S, \omega)$. The broken line indicates the classically expected value. Note the different vertical scales. (*a*) $S = 0.8$ and (*b*) $S = 1.0$.

the eigenfunctions corresponding to 'vague tori' and prevent a systematic dependence of $\bar{C}(E_S, \omega)$ on both the initial state and the Planck constant. In other words, the effects of quantum tunnelling (the tail) and the classical chaos (the 'vague tori') interfere with each other at $S = 0.8$. Thus we cannot identify any clear characteristics which can be attributed either to quantum tunnelling or the classical chaos. At $S = 1.0$ the fluctuation of the initial state dependence reduces to the non-logarithmic scale. This indicates that quantum tunnelling ceases to play a significant role and that the classical chaos becomes predominant. This is due to the appearance of 'ergodic' eigenfunctions discussed in § 3. However, these eigenfunctions are accompanied by quantum beats randomly distributed over the whole of the chaotic region. They produce non-logarithmic scale irregularities of the transition probabilities between the two primary resonances. Nevertheless, the relative number of 'ergodic' eigenfunctions gradually increases with the decrease of the Planck constant. Therefore, the classical ergodicity seems to be recovered although the magnitude of $\bar{C}(E_S, \omega)$ is still less than that expected classically (see figure 7(b)). In other words we characterise the situation as follows: each of the classical paths contributes to the leak of the probability out of the domain of the first primary resonance. However, the quantum probability distribution cannot closely follow the behaviour of the corresponding classical one due to the interference between classical paths. We can call such a property the 'partial ergodicity'.

In summary the statistical properties of the quantum system qualitatively reflect the classical transition to global chaos as follows: below the threshold the leak of the probability through KAM tori is due to pure quantum tunnelling. Just above the threshold the effects of quantum tunnelling and the classical chaos interfere with each other. Sufficiently far above the threshold the effect due to classical chaos is predominant and the classical ergodicity seems to be recovered.

5. Conclusion

We have investigated a quantum version of resonance overlap from various points of view.

Our most important discovery is that the phase space profile of the eigenfunctions reflects the stochasticity of classical chaos in their features of random quantum beats. Let us briefly summarise how these features of the eigenfunctions emerge with the advance of resonance overlap. Below the global stochastisation threshold, eigenfunctions correspond to quantised KAM tori and a hierarchy of eigenfunctions reflects the self-similar structure of higher-order resonances in the classical phase space. Just above the threshold eigenfunctions are localised in the phase space as they correspond to quantised 'vague tori' in which classical trajectories are confined for finite time intervals. However, qualitative features of quantised 'vague tori' are different from those of quantised KAM tori. The phase space profile of eigenfunctions is accompanied by lumps due to quantum interference. This stems from the fact that classical tori are damaged and bifurcated into multiple branches just above the threshold. Nearby, branches of a wavefunction on a multiply bifurcated torus interfere with each other to form slowly varying beats along the phase space profile of eigenfunctions. As resonance overlap advances further, these lumps due to quantum interference are distributed much more irregularly over much wider regions. Moreover, some eigenfunctions extend over the whole of the chaotic region although their relative number is limited. This is attributed to the appearance of chaotic global manifolds which have

complicated structures composed of infinitely multiplicate branches. On such a manifold, phase differences of a wavefunction between nearby branches become random. Thus a wavefunction interferes with itself to form lumps randomly distributed over the chaotic phase space. Therefore, the more stochastic the classical behaviour, the more complicated the quantum beat features. We propose that it is appropriate to call this phenomenon quantum chaos.

The statistical properties of the quantum system qualitatively reflect the classical transition to global chaos: below the threshold S_C the quantum probability leaks through KAM tori by quantum tunnelling. Just above the threshold the effects of quantum tunnelling and the classical chaos interfere with each other and we cannot identify any clear characteristics which can be attributed either to quantum tunnelling or to classical chaos. Moreover, we cannot find any tendency toward the recovery of the classical ergodicity. This is explained in terms of 'vague tori'. Sufficiently far above the threshold, the effect of classical chaos appears predominant. This is due to the appearance of global eigenfunctions which spread over the whole of the chaotic region. Further, the classical ergodicity seems to be recovered as the Planck constant becomes small.

Many questions remain to be answered. Among them are the following important ones. (i) How can we quantise chaotic manifolds semiclassically to obtain eigenfunctions? (ii) Do quantum systems exhibit statistical properties which reflect mixing in corresponding classical systems? (iii) What are the limitations of the classical–quantum correspondence in chaotic systems? How can we understand such limitations from a semiclassical viewpoint? (iv) How can we quantitatively characterise the complicated features of wavefunctions due to chaos? These problems will be studied in future publications.

Acknowledgment

We thank P Davis for critical reading of the manuscript and S Adachi for providing computer programs to display the phase space profile of the eigenfunctions.

Appendix

To obtain the stroboscopic transformation U defined by (3) we numerically integrate the time-dependent Schrödinger equation $i\partial\psi/\partial t = H(t)\psi(t)$. As a basis to represent the Schrödinger equation we choose the eigenfunctions $\{u_l\}$ of the momentum operator $I = -i\partial/\partial\theta$. Expanding as $\psi(t) = \Sigma_l a_l(t)u_l$ and transforming into the interaction representation $b_l(t) = \exp(-l^2 t/2i)a_l(t)$ we immediately obtain the equation of motion

$$(2i/V)\dot{b}_l(t) = (1+e^{-i\omega t})\exp[-i(l+\tfrac{1}{2})t]b_{l+1}(t) + (1+e^{i\omega t})\exp[i(l-\tfrac{1}{2})t]b_{l-1}(t). \qquad \text{(A1)}$$

We integrated (A1) numerically by the Adams method. In practice we truncated (A1) by setting $b_l(t) \equiv 0$ for l out of a relevant range of the momentum. Here we choose the relevant range two times wider than the classical chaotic region roughly given by $-2\sqrt{V} \leqslant l \leqslant \omega + 2\sqrt{V}$. Transforming back to the Schrödinger representation we numerically diagonalised U to obtain the eigenfunctions $\{\phi_k\}$ and the eigenvalues $\{\exp i\varepsilon_k\}$. We checked the unitarity of U by examining the orthonormality of the eigenfunctions $\{\phi_k\}$ obtained within the decimal of about 12 digits.

References

Berry M V 1977a *Phil. Trans. R. Soc.* A **287** 237
—— 1977b *J. Phys. A: Math. Gen.* **10** 2083
—— 1981 *Ann. Phys., NY* **131** 163
Casati G, Chirikov B V, Izrailev F M and Ford J 1979 *Stochastic Behavior in Classical and Quantum Hamiltonian Systems* (*Lecture Notes in Physics* **93**) ed G Casati and J Ford (Berlin: Springer) p 334
Chirikov B V 1979 *Phys. Rep.* **52** 265
Einstein A 1917 *Verhand. Deut. Phys. Ges.* **19** 82
Escande D F and Doveil F 1981 *J. Stat. Phys.* **26** 257
Fishman S, Grempel D R and Prange R W 1982 *Phys. Rev. Lett.* **49** 509
Greene J 1968 *J. Math. Phys.* **9** 760
—— 1979 *J. Math. Phys.* **20** 1183
Grempel D R, Prange R E and Fishman S 1984 *Phys. Rev.* A **29** 1639
Heller E 1984 *Phys. Rev. Lett.* **53** 1515
Ikeda K and Toda M 1983 unpublished
Jaffé C and Reinhardt W P 1982 *J. Chem. Phys.* **77** 5191
Korsh H J and Berry M V 1981 *Physica* **3D** 627
Lichtenberg A J and Lieberman M A 1983 *Regular and Stochastic Motion* (Berlin: Springer)
McDonald S W and Kaufman A N 1979 *Phys. Rev. Lett.* **42** 1189
Percival I C 1973 *J. Phys. B: At. Mol. Phys.* **6** L229
Shirts R B and Reinhardt W P 1982 *J. Chem. Phys.* **77** 5204
Takahashi K and Saito N 1985 *Phys. Rev. Lett.* **55** 645